Toxicology Letters 210 (2012) 293–301

Contents lists available at SciVerse ScienceDirect

Toxicology Letters

journal homepage: www.elsevier.com/locate/toxlet

Distinct immunomodulatory effects of a panel of nanomaterials in human dermal fibroblasts

Amelia A. Romoser[a], David E. Figueroa[a], Aishwarya Sooresh[b], Kelly Scribner[a], Patricia L. Chen[c], Weston Porter[a,e], Michael F. Criscitiello[a,c,**], Christie M. Sayes[a,d,f,*]

[a] Interdisciplinary Program of Toxicology, Texas A&M University, College Station, TX 77843, United States
[b] Interdisciplinary Program in Material Science & Engineering, Texas A&M University, College Station, TX 77843, United States
[c] Department of Veterinary Pathobiology, Texas A&M University, College Station, TX 77843, United States
[d] Department of Veterinary Physiology & Pharmacology, Texas A&M University, College Station, TX 77843, United States
[e] Department of Veterinary Integrative Biosciences, Texas A&M University, College Station, TX 77843, United States
[f] Department of Biomedical Engineering, Texas A&M University, College Station, TX 77843, United States

ARTICLE INFO

Article history:
Received 27 November 2011
Received in revised form 24 January 2012
Accepted 25 January 2012
Available online xxx

Keywords:
Quantum dots
Titanium dioxide
Silver
Fullerol
Nanoparticles
NF-κB pathway

ABSTRACT

There are many efforts in understanding the effects of nanoparticles on cell viability and metabolism, however, not much is known regarding the distinct molecular mechanisms of inflammation and cellular stress using low dosing concentrations. To address this gap in the literature, we utilized a novel experimental design that specifically probes the effects of a panel of commonly studied engineered nanomaterials along immunomodulatory pathways, including NF-κB. The panel of particles selected for this study included quantum dot nanocrystals, titanium dioxide, hydroxylated fullerenes, and silver nanoparticles. Cell viability, antioxidant activity, select messenger RNA, and protein modulation were studied in primary human dermal fibroblasts (HDF) and NF-κB knockdown HDF cells. Inflammatory and non-inflammatory immune responses were measured using protein and real-time PCR array analysis from HDF cells exposed to sub-lethal concentrations of nanoparticles. Differences in cellular response to nanoparticles in protein and antioxidant experiments were evident in NF-κB knockdown cells. The methods used in the study, along with the resultant data sets, serve as a potential model for studying the complex pathway-specific biochemical responses in cell and tissue systems associated with nanoparticle exposures.

1. Introduction

There has been rapid progress in the field of nanotoxicology in recent years; however, information regarding the potential for adverse health outcomes arising from nanoparticle exposures is still lacking. For example, the cellular immunoregulatory response to nanoparticles is not well understood. Materials on the nanometer size scale are thought to impose different types of chemical and/or biological effects on organisms compared to materials of the same chemical composition but on the micrometer size scale. This phenomenon is attributed to the finer size and corresponding larger surface area per unit mass that is characteristic of all engineered nanoparticles (Maynard and Kuempel, 2005; Monteiller et al., 2007; Oberdorster et al., 2005). However, it is largely unknown which specific pathways or subcellular mechanisms of action are triggered as a result of nanoparticle exposure. Some studies have shown that nanoparticles can be internalized into cells. Other studies have shown various uptake mechanisms for nanoparticles (Duan and Nie, 2007; Jaiswal et al., 2003; Zhang and Monteiro-Riviere, 2009). But few studies have investigated the subsequent mechanisms of injury, including key genes and proteins that participate on the molecular level. A key missing component of most nanotoxicology studies is the query and determination of toxicological process development. We hypothesized that immune mediators of inflammation, such as the transcription factor, NF-κB, may be initiated in the exposed cell layers, and followed by upregulation of inflammatory response proteins. NF-κB may be partially affected by MAPKs, such as ERK1/2 and p38, which are known to phosphorylate the NF-κB inhibitor (Müller et al., 2002). We have found that these initiators are, at least in part, dependent on nanoparticle type and the cellular stress response ability of the cell.

* Corresponding author at: Center for Aerosols and Nanomaterials Engineering, RTI International, Research Triangle Park, NC 27709, United States. Tel.: +1 919 541 6414; fax: +1 919 541 6936.
** Corresponding author at: Department of Veterinary Pathobiology, Texas A&M University, College Station, TX 77843, United States. Tel: +1 979 845 4207; fax: +1 979 862 1088.
E-mail addresses: mcriscitiello@cvm.tamu.edu (M.F. Criscitiello), csayes@rti.org (C.M. Sayes).

0378-4274/$ – see front matter © 2012 Elsevier Ireland Ltd. All rights reserved.
doi:10.1016/j.toxlet.2012.01.022

We previously showed that quantum dot exposure modulates NF-κB in human dermal fibroblasts (HDFs) (Romoser et al., 2011). NF-κB is a major transcription factor responsible for regulating genes of both the innate and adaptive immune responses (Livolsi et al., 2001). NF-κB becomes activated through distinct signaling components: inactivated, cytosolic NF-κB is complexed with the inhibitory IκBα (NFKBIA) protein. A variety of extracellular signals can be recognized via integral membrane receptors, which can lead to the activation of the enzyme IκB kinase (IKK or IKBKB). The role of IKK is to phosphorylate the NF-κB-associated IκBα protein, resulting in ubiquination and dissociation of IκBα from NF-κB. IκBα is degraded by the proteosome and the liberated NF-κB is then translocated into the nucleus where it binds to specific DNA motifs in promoters, termed response elements. Here, it can upregulate genes involved in immune cell development, and maturation, as well as those dedicated to survival, inflammation, and lymphoproliferation (Zandi, 1997).

In an attempt to elucidate these immune response mechanisms, primary HDF cells were utilized to investigate the molecular toxicological mechanisms of a collection of similarly sized nanoparticles. Fibroblasts are the most common cell-type in the dermis, and their ubiquity makes them more appropriate for this study than the rare patrolling macrophages. Contact with the skin is one of the major routes of both intentional and accidental exposures to nanoparticles. Four dermally relevant nanoparticles, citrate-stabilized silver, hydroxylated fullerenes (fullerol), CdSe/ZnS-COOH quantum dots, and anatase titanium dioxide, were chosen to compare and contrast cellular responses.

Because of their unique characteristics, quantum dots are used at increasing rates for a wide variety of industrial and consumer-based applications, including biomedical imaging agents, inks, and solar panels (Alivisatos et al., 2005; Gao et al., 2004; Michalet et al., 2005; Roco, 2003). Zhang and Monteiro-Riviere (2008) and Mortensen et al. (2008) both concluded that quantum dots of similar or identical structure and composition to those used in this study could penetrate through the epidermis into the dermis, especially with flexing of the skin or by way of hair follicles. Microscopy from their publications revealed that a considerable portion of the dose penetrated to the dermis. Silver is currently being utilized as an antimicrobial agent in many dermal applications and has been found to penetrate intact and damaged skin (Larese et al., 2009; Samberg et al., 2010). Titanium dioxide, a common ingredient in sunscreens and cosmetics, is generally recognized as safe for dermal exposure. However, while most titanium dioxide studies involving healthy skin report an absence of penetration, this may not necessarily be the case with damaged skin (Tamura et al., 2010; L'Oreal unpublished study – 2009–2011). We also examined the effects of fullerol exposure on dermal cells in this study. Fullerol has been reported to possess antioxidant abilities (Djordjevic et al., 2005; Mirkov et al., 2004; Wang et al., 1991) and has, for that reason, been added to cosmetic preparations with the intention of preventing oxidative damage to the skin due to aging and sun exposure. But there have also been reports of toxicity associated with exposure to fullerol and other carbonaceous cage nanostructures. For example, Xia et al. (2010) have recently reported that, depending on the vehicle composition, pristine fullerene nanoparticles can penetrate deeply into the stratum cornea in healthy skin, as tested both *in vitro* and *in vivo* (Xia et al., 2010). In another study, fullerol caused delayed cell death characteristic of apoptosis, including DNA damage in rodent and human glioma cells, which was determined to be caused in the absence of ROS (Isakovic et al., 2006). The dermal permeation capability or toxicity of fullerol, specifically, has not been assessed, although fullerene-based peptides were shown to penetrate intact skin, which was exaggerated with mechanical stress leading to infiltration into the dermis (Rouse et al., 2007).

In an effort to increase current knowledge regarding pathways of the human cellular response to aqueous silver, fullerol, quantum dots, and titanium dioxide, we have quantitatively investigated effects of exposure on the expression of 84 unique genes in HDF cell cultures. In this study, we compared the dose–response and time-course effects of four nanoparticles in dermal cells capable of exhibiting inflammatory response, immunoregulation, apoptosis, and cellular stress. Additionally, we tested whether NF-κB was modulated, as was found in our previously published study (Romoser et al., 2011), in cells exposed to other nanoparticles and determined to what extent NF-κB played a role in the cellular response to NPs by overexpressing the inhibitor, IκBα. We have included an experimental design flowchart that outlines all experiments carried out (Supplemental Fig. 1).

2. Methods

2.1. Nanoparticle characterization

Aqueous citrate-stabilized silver particles (NanoComposix, San Diego, CA), hydroxylated fullerenes (MER Corp., Tucson, AZ), CdSe/ZnS-COOH crystalline quantum dots (Invitrogen Corp., Carlsbad, CA), and anatase titanium dioxide (NanoAmor, Houston, TX) characterization data are summarized in Table 1. The hydrodynamic diameter and zeta potential of all four nanoparticles were measured using a Zeta Sizer Nano Series ZEN 3600 Spectrometer (Malvern Instruments Ltd, Malvern, Worcestershire, UK). Particle characterization was performed on the particles suspended in Milli-Q ultrapure water (18.2 mΩ), as well as in DMEM supplemented with 10% FBS at 0, 24, and 48 h time points. Elemental analyses were determined via inductively coupled plasma-mass spectroscopy (Elan DRC II, Perkin Elmer SCIEX). Transmission electron microscopy (TEM) grids were glow discharged using PELCO easiGlow (Ted Pella, Inc., Redding, CA) in order to make the grid surface hydrophillic. Fifteen microliters of solution was applied to 200 lines/inch square mesh copper grids (Electron Microscopy Sciences, Hartfield, PA). Grids were analyzed on a FEI Tecnai G2 F20 at an accelerating voltage of 200 kV. Images were recorded using a Gatan CCD camera.

2.2. Cell culture and experimental dosing

2.2.1. Human dermal fibroblasts

Cryopreserved primary HDF cells (PCS-201-010, ATCC, Manassas, VA) were cultured in Dulbecco's Modified Eagle's Medium supplemented with 10% FBS (Gibco, Austria). Media was supplemented with an antibiotic cocktail consisting of penicillin, streptomycin, and amphotericin (Sigma–Aldrich, St. Louis, MO). Incubation took place at 37 °C with humidity and 5% CO_2. Cells were grown to 80% confluency in 6-well plates, then exposed to nanoparticles (20 ppm final exposure concentrations) or untreated for a negative control. Cells treated with nanoparticle suspensions were very briefly exposed to light in the cell culture hood at the points of exposure and harvesting. Cellular incubations with nanoparticles took place in the dark.

2.2.2. Stable transduction of HDF cells

An additional group of HDF cells was virally transduced to overexpress IKBα, the inhibitor of NF-κB, to assess differences in viability, antioxidant usage, and protein expression with and without NF-κB competency. HEK-293T Ampho-Phoenix packaging cells, capable of carrying plasmids for long-term stable production of lentivirus, were obtained with permission from Gary Nolan at Stanford University and maintained in DMEM containing 10% FBS at 37 °C with 5% CO_2. HDF cells were maintained as aforementioned. This transduced HDF cell line is referred to as "NF-κB knockdown" cells throughout the manuscript.

2.2.3. Construction of plasmid

IκB-SR (Super Repressor) was amplified with primers 5′-ATG TTC CAG GCG GCC GAG-3′ and 5′-TCA TAA CGT CAG ACG CTG GC-3′, cloned onto pCR2.1 TOPO (Invitrogen) and subcloned onto pLPCX (Clontech) using *EcoRI* restriction sites.

2.2.4. Stable transduction in cell lines

HEK-293T amphotrophic Phoenix cells were transfected with 10 μg retroviral vectors (pLPCX) with or without insert. After 24 h, cells were placed at 32 °C. Viral media was harvested 48 and 72 h after transfection and used to infect cells. After 24 h of resting in nonselective media, cells were selected with 0.4 μg/mL puromycin for 48 h. Empty vector does not appreciably alter gene expression profile. Real-time PCR compared expression of genes from cells treated with empty vector (no NF-κB construct) to the cells that received no nanoparticle and were harvested at 8 h (data not shown).

Table 1
Characterization table.

Characterization			Silver		Fullerol		QD		TiO_2
Primary particle size reported by manufacturer (nm)			25		15		16		25
Primary particle size measured by TEM (nm)			20		–		10		15
Density (g/cm^3)			10.50		0.80 (fullerene)		4.95 (CdSe/ZnS)		3.90
	Water	Media	Water	Media	Water	Media	Water	Media	
Size measured by DLS (nm)									
0 h	54 ± 2	169 ± 2	239 ± 9	102 ± 5	13 ± 0	27 ± 1	40 ± 3	314 ± 63	
24 h	354 ± 23	123 ± 4	31 ± 1	121 ± 5	23 ± 2	23 ± 1	156 ± 29	17 ± 1	
48 h	345 ± 3	166 ± 3	31 ± 0	195 ± 4	39 ± 8	25 ± 1	1332 ± 540	249 ± 150	
Zeta potential (mV)									
0 h	−48 ± 9	−9 ± 2	−51 ± 7	−13 ± 1	−51 ± 6	−4 ± 1	+42 ± 8	−11 ± 1	
24 h	−55 ± 2	−10 ± 1	−10 ± 5	−15 ± 1	−8 ± 3	−1 ± 0	+11 ± 1	−12 ± 1	
48 h	−56 ± 3	−11 ± 1	−27 ± 3	−15 ± 0	−39 ± 7	−5 ± 1	−0.5 ± 0	−13 ± 0	

Nanoparticle size as measured by manufacturer, TEM, and dynamic light scattering, zeta potential, and density of silver, fullerol, quantum dots, and titanium dioxide.

2.3. Cell viability

HDF and NF-κB knockdown cells were cultured in 24-well plates as described above. Cells were then exposed to silver, fullerol, quantum dots, or titanium dioxide to give final well concentrations of 0, 10, 50, 100, 150, or 200 ppm. Cells treated for 24 or 48 h were washed, trypsinized, and resuspended in cell culture media. Percentages of viable cells were measured by mixing equal volumes of cell suspension and trypan blue stain, followed by membrane permeability-based counting in an automated cell counter (Countess, Invitrogen). Viability experiments were done in quadruplicate. For HDF cells, a student's *t*-test was employed using GraphPad software to calculate significant change in viability for each particular treatment, as compared to the untreated control samples. Similar statistical analysis was performed for the case of NF-κB knockdown cells.

2.4. GSH oxidation assay

A luminescence-based assay (V6611, Promega, Madison, WI) was utilized to detect and quantify levels of glutathione disulfide (GSSG) in both untreated and 20 ppm nanoparticle-treated HDF and NF-κB knockdown cells. GSSG determinations were based on a reaction scheme consisting of GSH-dependent conversion of a GSH probe to luciferin by a glutathione S-transferase enzyme. Both GSH and GSSG are present in cells. Therefore, in order to measure glutathione disulfide only, cells were lysed and GSH was blocked. The resulting GSSG was reduced to GSH to measure glutathione disulfide. Antioxidant experiments were done in triplicate. A student's *t*-test was employed to calculate significant change in viability for each particular treatment in HDF cells, as compared to the untreated control samples. Similar statistical analysis was performed for the case of NF-κB knockdown cells. Pair wise analysis was also performed in a similar manner for each particular treatment scenario, where the NF-κB knockdown cells were compared to the HDF cells.

2.5. Gene expression analysis

Cells cultured and exposed to 20 ppm nanoparticle suspensions were harvested at time points of 8 or 24 h. An RNeasy® Mini Kit (Qiagen, Frederick, MD) was used in conjunction with an on-column genomic DNA digestion to lyse cells and extract total RNA. An RT^2 First Strand Kit (C-03) from SABiosciences was utilized prior to quantitative real-time PCR (RT-PCR) to reverse transcribe messenger RNA into cDNA. This cDNA was prepared for a pathway-focused gene expression profiling PCR array system, specific for 84 genes of innate and adaptive immune responses (RT^2 Profiler™, SABiosciences, Frederick, MD), of which data from 42 passed quality control in all conditions are compared here. After adding the cDNA to a PCR reaction master mix containing SYBR green, 25 μL of sample was loaded into all wells of 96-well plates pre-filled with primer sets including housekeeping genes, gDNA controls, reverse transcription controls, and positive PCR controls. One plate was assayed for each experimental condition. Using a Roche LightCycler® 480 (Roche, Indianapolis, IN) for RT-PCR, a two-step thermal cycling program was followed: 1 cycle at 95 °C for 10 min, then 45 cycles of 95 °C for 15 s, then 60 °C for 1 min. The Roche LightCycler® 480 software was utilized for raw data acquisition and calculation of Ct (threshold cycle) values.

2.6. Protein expression alteration

HDF and HDF transduced with empty vectors (i.e. no IκBα overexpression capability) were cultured in the same conditions as above. Nanoparticle-treated and untreated cells were washed in ice cold 1× PBS, then protease inhibitor cocktail (Sigma–Aldrich) and high salt lysis buffer were added to wells. Protein was isolated by collecting supernatant via centrifugation. Fractionated NF-κB samples were harvested without the use of lysis buffer. An NF-κB activation assay kit (FIVEphoton Biochemicals, San Diego, CA) was utilized to obtain nuclear and cytosolic NF-κB fractions from cells. Samples were loaded into 10% SDS-PAGE gels and run at 120 mV. Gels were transferred to PVDF membranes, which were blocked in 5% milk or BSA/PBST and incubated in different primary antibody solutions overnight: p-IκBα, 1:1000 (Abcam Inc., Cambridge, MA); p-ERK1/2, 1:1000 (Cell Signaling Technology, Danvers, MA); HMOX-1, 1:1000 (Santa Cruz Biotechnology, Santa Cruz, CA); p-P38, 1:1000 (Cell Signaling Technology); IL-6, 1:500 (Santa Cruz); or p65 NF-κB, 1:1500 (Santa Cruz). Membranes were washed in PBST several times before secondary antibody (Goat, anti-mouse or anti-rabbit, 1:5000, Santa Cruz) prepared in fresh 5% milk or BSA/PBST solution was added. Membranes were incubated in the secondary antibody at room temperature, and then washed again in PBST. Immobilon™ Western Chemiluminescent HRP substrate (Millipore, Billerica, MA) was added to membranes and film exposures were taken. GAPDH, 1:10,000 (AM4300, Ambion, Austin, TX) and Lamin A/C 1:5000 (sc-6215, Santa Cruz) were used as loading controls. Blots are representative of duplicate or triplicate experiments. Densitometric analysis of western blot results can be found in Supplemental Figs. 4 and 5. Statistical analysis was performed using a student's *t*-test to calculate significant change in expression for each particular treatment, as compared to the untreated control samples. Similar statistical analysis was performed for the case of NF-κB knockdown cells. Pair wise analyses were also made using this test for each particular treatment scenario, where the NF-κB knockdown cells were compared to the HDF cells.

2.7. Calculations of gene expression changes

A total of five housekeeping (potential reference) genes were assayed on the plate and included those encoding β_2-microglobulin, hypoxanthine phosphoribosyltransferase 1, ribosomal protein L13a, glyceraldehyde-3-phosphate dehydrogenase, and β-actin. Analytical estimation of internal control gene stability indicated that hypoxanthine phosphoribosyltransferase 1 (*HPRT1*) was most stable based upon lowest variance and standard deviation, and *HPRT1* was utilized for subsequent normalization (Vandesompele et al., 2002).

Changes in gene expression were estimated using the $2^{-\Delta\Delta Ct}$ method (Ryman-Rasmussen et al., 2007; Rzigalinski and Strobl, 2009), with *HPRT1* utilized as the stable reference gene for all experimental situations. The fold changes in gene expression were calculated with respect to the expression level of the genes in the respective control group. For example, 2-fold change of gene A indicates that expression of gene A was twice as large in the treatment group compared to its expression in the control group, while 0.5-fold change of gene A indicates that the expression of that gene was two times less in the treatment group compared to its expression in the control group. More detailed gene annotations and array layout are available at http://www.sabiosciences.com/genetable.php?pcatn=PAHS-065A. Information regarding the manufacturer's estimates for array performance, sensitivity, specificity, and reproducibility are available at http://www.sabiosciences.com/rt_pcr_product/HTML/PAHS-052A.html#accessory.

3. Results

3.1. Nanoparticle characterization

Nanoparticle characterization results can be found in Table 1, Fig. 1, and Supplemental Fig. 3. Primary particle size and morphology for all nanoparticles were determined via transmission electron microscopy; dynamic light scattering was utilized to measure the hydrodynamic diameter of the particles when suspended in water and complete cell culture media. Specific results can be found in Table 1. Lastly, the densities of the particles are reported to be 3.90 g/cm^3 for titanium dioxide, 10.50 g/cm^3 for silver, 4.95 g/cm^3

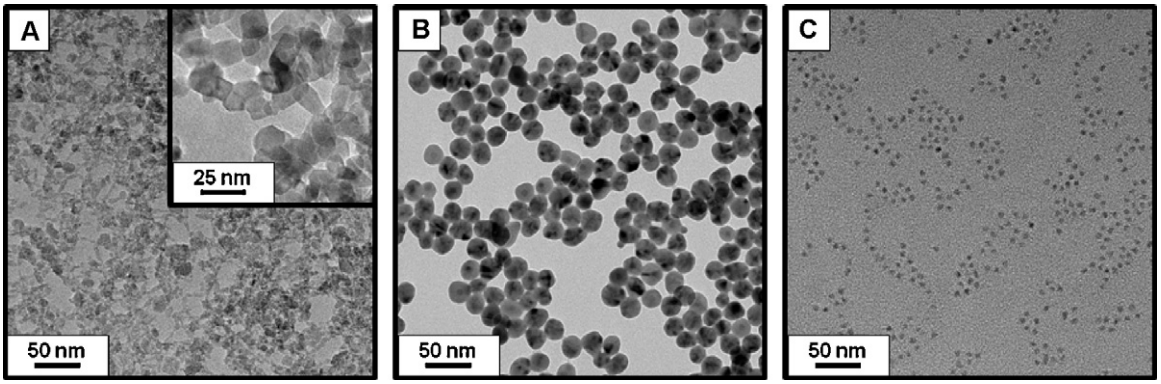

Fig. 1. Transmission electron microscopy: (A) titanium dioxide, (B) silver, and (C) quantum dots. Samples were diluted to 20 ppm in Milli-Q water. Characterization was done in cell-free conditions.

for CdSe quantum dots, and 0.80 g/cm^3 for fullerols. No metal impurities were detected via inductively coupled plasma-mass spectroscopy elemental analysis.

The hydrodynamic size of the particles, as measured by dynamic light scattering, changed over time for three of four particle types: the silver and TiO_2 particles became larger; the fullerol particles became smaller; and the quantum dot particles remained the same. In media, however, each particle maintained their aggregated size over time – all of which were larger than the size in water, except for the quantum dots. The surface charge of the particles, as measured by zeta potential, also changed over time for three of the four particle types: fullerol and quantum dot particles became less negative; TiO_2 become less positive; and the silver particles generally stayed the same. In media, however, each particle type maintained its slightly negative surface charge over time.

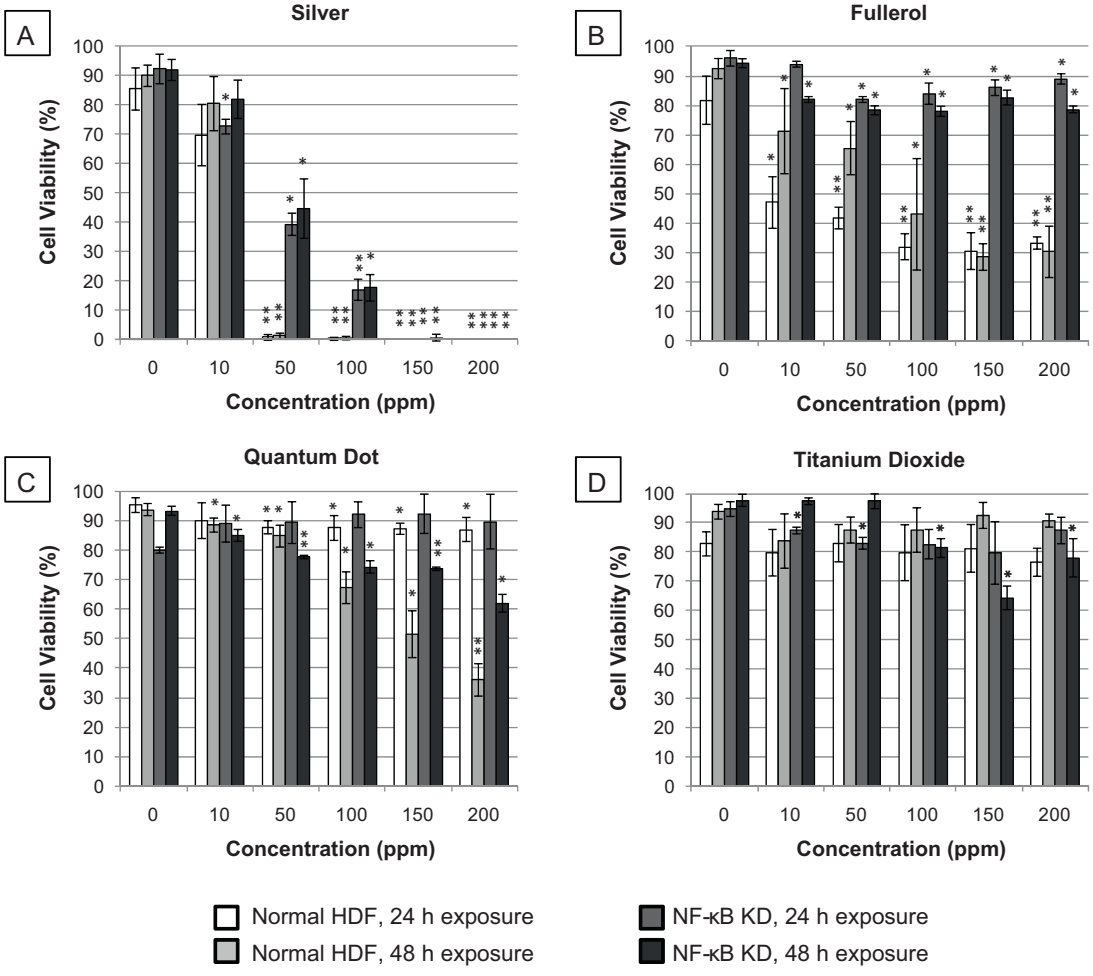

Fig. 2. Viability. Comparison of normal and NF-κB knockdown HDF cellular viability, as measured with the trypan blue exclusion assay. Measurements were taken 24 and 48 h after exposure to 0–200 ppm (A) silver, (B) titanium dioxide, (C) fullerol, or (D) quantum dots. *Statistically significant ($p < 0.05$) compared to untreated, cell-type matched cells. **Statistically significant ($p < 0.001$) compared to untreated, cell-type matched cells.

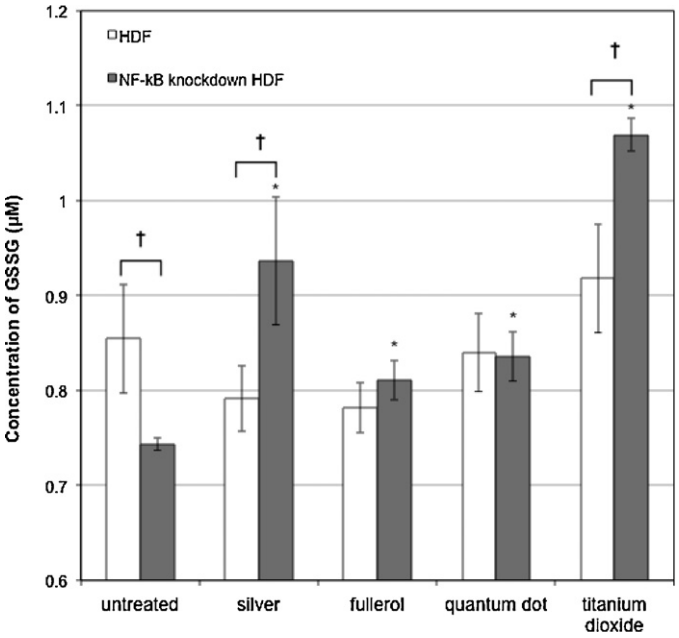

Fig. 3. GSH conversion. Glutathione disulfide was measured in normal and NF-κB knockdown HDF cells after 20 ppm nanoparticle treatment for 1 h. Responses from untreated cells were also included for comparison purposes. The assay is based on a luciferin conversion reaction catalyzed by glutathione-S-transferase. *Statistically significant ($p < 0.05$) compared to untreated, cell-type matched cells. †Statistically significant ($p < 0.05$) compared to normal HDF, treatment-matched cells.

3.2. Cell viability

Cellular viability was measured in HDF cells exposed to each nanoparticle over a dose–response ranging 0 to 200 ppm resulting in a differential cytotoxicity for each particle (Fig. 2). The trypan blue assay revealed that cell viability decreased (increase in membrane permeability) with increasing concentration of nanoparticle exposures. In addition, the cellular response to particles was found to be different when NF-κB was inhibited in cells. Specifically, the knocked down cells were generally more robust after exposures than normal HDF cells. Conversely, NF-κB knockdown cells were more sensitive to titanium dioxide than normal cells. In normal HDF cells, viability was affected more severely compared to untreated HDF cells when treated with silver, fullerol, or quantum dots. Increasing exposure time to 48 h with quantum dots, fullerols, and titanium dioxide also negatively affected viability, when compared to cells exposed for 24 h. Western blotting of nuclear and cytoplasmic fractions confirmed lack of NF-κB translocation in knock-down cells compared to empty vector (Supplemental Fig. 2).

Regarding the possibility of the citrate stabilizer in the silver material we used to generate additional cellular toxicity, Uboldi et al. (2009) recently concluded that sodium citrate concentrations as high as 0.7 mM resulted in only mild toxicity by 72 h continuous exposure (viability 70%). They found their data to be consistent with other findings regarding the use of sodium citrate to stabilize nanoparticle suspensions (Connor et al., 2005; Shukla et al., 2005).

3.3. Glutathione oxidation assay

Glutathione (GSH) plays an important role in antioxidant defense in eukaryotic cells. To assess antioxidant response after nanoparticle exposures, GSSG was measured in normal and NF-κB knockdown cells after 20 ppm nanoparticle treatment for 1 h (Fig. 3). Responses from untreated cells were also included for comparison purposes. Knocked down cells exhibited a greater antioxidant response after 1 h than normal cells when exposed to nanoparticles. Silver and titanium dioxide caused more GSH oxidation compared to fullerol and quantum dot-treated cells. This finding indicates that NF-κB plays a substantial role in antioxidant generation after nanoparticle exposures. GSH experiments were done in quadruplicate.

3.4. Gene expression analysis

In general, the 24 h time point revealed much higher upregulation of immune response related genes after nanoparticle exposures (Fig. 4). This trend was opposite for HMOX1 and TLR3, however. Upregulation of genes was similar between particle types, except for HMOX-1, which was only significantly upregulated with silver exposures. IL-1 family proteins were influenced most. Upregulation of IL-1 family and other genes in normal cells exposed to nanoparticles occurred at 24 h, with the exception of HMOX-1, which was induced at 24 h, but even more so at the earlier 8 h time point. The robust response of IL-1α and IL-1 family member 7 messages after prolonged exposure shows preparation for inflammation.

3.5. Protein expression alteration

As determined via western blot, NF-κB knockdown cells inhibit NF-κB nuclear translocation, preventing subsequent DNA binding and genetic upregulation; therefore, these cells were determined to be appropriate to assess the role of NF-κB after nanoparticle exposures (Supplemental Fig. 2). Real-time PCR analysis of immune gene mRNA levels of cells treated with the empty pLPCX retroviral vectors confirmed that the gene knockdown system was not altering genes itself (data not shown).

In assessing early transcription factor involvement, the severity of the NF-κB/ERK response in nanoparticle-treated cells is as follows: silver > fullerol > quantum dot > titanium dioxide. ERK1/2 upregulation either precedes or is nearly concurrent with phosphorylation of the NF-κB inhibitor, IκBα, in silver, fullerol, and titanium dioxide-treated cells, but not quantum dot-treated cells (Fig. 5). Suppression of IκB phosphorylation suggests that NF-κB inhibition occurs. Induction of phosphorylated p38 is seen at both time points after exposure to all four nanoparticle types.

To analyze downstream protein response arising from perturbation of earlier transcription factor modulation, we probed for induction of phosphorylated p38, HMOX-1, and IL-1α (Fig. 6). Phosphorylated p38 expression was evident after exposure to all four nanoparticle types, but was notably less severe with NF-κB knockdown. HMOX-1 expression was limited to silver-treated cells, indicating ROS generation and resistance to protein damage. By 24 h, knockdown cells reveal less HMOX-1 induction. P38 and HMOX-1 results indicate that 24 h exposure with silver and quantum dots causes partial dependency upon NF-κB for oxidative stress-related signaling. IL-1α blots suggest that NF-κB is responsible for controlling much of the inflammatory response in the dermal cells tested.

4. Discussion

Specific, pathway-driven cellular responses to nanoparticle exposures need to be further elucidated for improved drug delivery, immune/inflammatory response mechanism elucidation, and gathering of basic toxicological response data. Studies comparing multiple nanoparticle types and probing for specific uptake mechanisms and distinct signaling pathway responses are needed to assess the effects of altering unique physicochemical characteristics of particles, such as chemical composition, size, and surface charge on appropriately dosed cell and tissues in culture.

8 h					24 h			
Silver	Fullerol	Quantum Dot	Titanium Dioxide		Silver	Fullerol	Quantum Dot	Titanium Dioxide
0.42	1.03	0.63	0.81	**ADORA2A**	0.67	--	0.74	0.41
0.79	1.21	1.01	1.03	**C5**	0.82	1.77	1.12	1.45
0.68	0.80	0.87	0.94	**CASP1**	1.20	1.71	1.40	1.06
1.18	0.85	0.88	1.05	**CASP4**	1.28	1.27	1.00	1.03
0.81	0.62	0.77	0.88	**CCL2**	0.96	0.82	1.07	1.36
1.12	1.01	1.01	1.05	**CD55**	1.94	2.26	1.50	0.95
0.95	0.63	0.77	0.84	**CHUK**	1.76	1.59	1.28	0.77
0.65	1.13	0.93	0.96	**COLEC12**	0.88	1.44	0.97	0.81
0.55	1.11	0.92	1.14	**FN1**	1.69	2.24	1.76	1.73
27.63	1.13	0.74	0.80	**HMOX1**	11.16	1.79	1.48	0.63
0.48	0.96	0.86	1.01	**IFNA1**	1.13	1.34	1.46	2.16
0.95	1.02	0.69	0.92	**IFNGR1**	1.31	1.62	1.49	1.33
0.91	0.76	0.87	0.82	**IFNGR2**	0.90	1.70	1.73	1.42
0.92	1.20	1.00	1.14	**IKBKB**	1.12	2.26	1.15	1.68
0.79	1.23	0.50	1.34	**IL10**	1.46	1.08	0.68	1.90
0.60	1.26	1.36	0.79	**IL1A**	5.13	2.26	2.37	2.18
0.78	0.80	0.55	1.09	**IL1B**	4.24	1.90	1.26	2.26
0.28	1.32	0.97	0.52	**IL1F7**	29.50	14.73	13.96	36.11
0.65	0.83	0.86	0.93	**IL1R1**	0.63	1.56	1.17	0.96
0.92	1.66	1.03	1.36	**IL1RAP**	1.99	2.39	1.33	2.13
1.11	0.65	0.99	0.56	**IL1RL2**	0.40	1.64	1.09	1.20
1.52	0.81	0.88	0.77	**IL6**	2.64	2.42	1.58	1.08
0.89	1.20	1.18	1.88	**IRAK1**	2.71	2.29	3.19	3.20
0.77	0.58	0.70	0.64	**IRAK2**	1.39	0.63	0.74	0.82
0.76	1.30	0.82	1.21	**IRF1**	0.77	1.54	1.45	1.81
0.84	1.05	0.85	1.04	**LY96**	1.82	1.24	1.09	0.90
0.73	1.05	0.92	1.15	**MAPK14**	1.26	1.58	1.48	1.51
0.78	0.85	0.94	0.94	**MAPK8**	1.56	1.81	1.58	1.63
0.94	1.20	1.00	1.16	**MIF**	1.67	1.35	1.09	0.90
0.77	1.18	1.18	1.34	**MYD88**	1.25	1.74	1.45	1.78
0.90	0.90	0.95	0.90	**NFKB1**	1.47	1.30	1.16	0.80
0.72	1.29	1.14	1.29	**NFKB2**	1.18	1.77	2.21	1.36
1.12	1.03	0.95	1.00	**NFKBIA**	1.01	1.11	1.11	0.65
0.37	0.52	0.81	0.53	**NLRC4**	1.91	2.59	1.99	0.55
0.79	1.09	0.80	1.08	**SERPINE1**	0.98	1.47	0.88	1.30
0.87	1.03	1.01	1.14	**TGFB1**	0.94	1.55	1.62	1.77
1.17	2.59	1.80	1.92	**TLR3**	0.74	1.42	1.38	0.84
1.13	0.85	0.93	0.99	**TLR4**	1.09	1.01	0.95	0.87
1.09	1.84	1.36	0.97	**TLR6**	1.28	1.87	1.38	1.28
0.90	1.11	0.90	1.00	**TNFRSF1A**	0.84	1.13	0.86	0.37
1.16	0.71	1.02	0.75	**TOLLIP**	1.39	1.32	1.22	0.65
1.13	0.77	0.98	0.79	**TRAF6**	1.37	1.58	1.38	0.92

Fig. 4. Immune gene expression. Heat map of pathway-specific gene expression changes in normal HDF. Central column shows genes in bold, columns to the left and right show fold change in expression levels in response to the 20 ppm treatment (labeled at top), compared to untreated controls assessed at the same time point (8 or 24 h). Fold suppressions of <0.5 are colored dark green and 0.5–0.8 light green. Fold inductions of 1.2–2.0 are pink and >2.0 red. (For interpretation of the references to color in this figure legend, the reader is referred to the web version of the article.)

This research describes a unique systematic investigation designed to assess the impact of a key inflammatory response mediator, namely NF-κB, after exposure to a panel of nanoparticle types in human skin cells. It is important to note that the cell type used in the assays was primary in nature, thus the results reported in this study are a better representation of an *in vivo* hazard assessment when compared to results obtained from an immortalized cell line. In an *in vivo* dermal exposure, the first line of defense is the epidermal layer of the skin, followed by the underlying dermal layer. In homeostasis, this layer of the skin consists of primarily fibroblasts and very few wandering Langerhans cells. Fibroblast cultures represent the sentinel cells in an animal. Langerhans cells, even if activated, do not persist in this area. Fibroblasts will remain intact in the dermis, as they reside in this location. Lastly, these studies were conducted using very low doses and, thus, may be more physiologically relevant than results from studies that use higher dosing concentrations.

A summary of experiments is outlined in an experimental flowchart (Supplemental Fig. 1). The chart describes experiments with normal, primary HDF cells and experiments carried out with virally transduced NF-κB knockdown HDF cells. We utilized a step-wise approach, beginning with coarse analyses of viability and antioxidant depletion. Then, we examined the finer analyses of gene and protein modulation. Investigations with knockdown cells were critical to determine the amount of NF-κB contribution after treatments, therefore helping to elucidate one of the primary immune and inflammatory response mechanisms in nanoparticle exposures. By analyzing resultant response data, we were able to make several speculations regarding the relationship between nanoparticle characteristics and cellular stress or inflammatory response outcomes.

The characteristics of every particle type used in these studies were measured for size and agglomeration state, surface charge, purity, density, and crystallinity. These particles were selected because they were (1) produced in the liquid phase with specific surface modifications to remain as suspensions in the aqueous phase for longer than 30 days on the shelf and (2) engineered to be of equivalent primary particle size. The silver particles were citrate stabilized, the fullerols were fully hydroxylated, the quantum dots were modified with carboxyl acid groups, and the titanium dioxide particles were functionalized with acetic acid groups. While these particles were designed to be water-suspendable and intended to remain at a primary size of ~20 nm, the physiologic fluid (i.e. cell culture media) significantly changed the zeta potential of the particles. The change in zeta potential influenced a change in the suspension iso-electric point, which is defined as the pH at which a particle has no net charge. Changes in iso-electric point cause particles that, under ultrapure water conditions, are normally

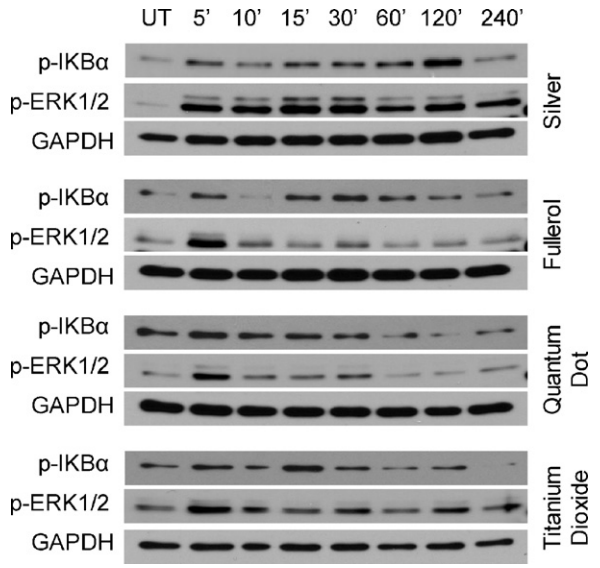

Fig. 5. Early transcription factor stimulation. To determine nanoparticle-specific differences in early transcription factor modulation, NF-κB inhibitor, IKBα, and ERK1/2 MAP kinase modulation in normal HDF were assessed after 20 ppm nanoparticle exposure over 5–240 min. Blots are grouped by nanoparticle type. GAPDH assured equal protein loading. Blots are representative of three identical experiments.

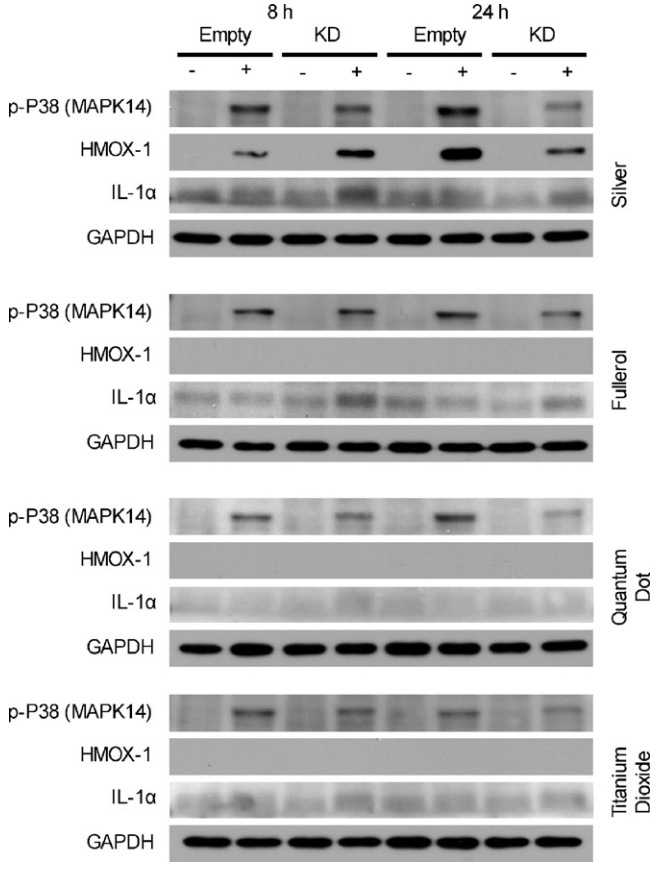

Fig. 6. Downstream protein expression. Western blot analysis of NF-κB pathway-related protein expression after 8 and 24 h exposure to 20 ppm silver, fullerol, quantum dot, and titanium dioxide. Phosphorylated p38, HMOX-1, and IL-1α protein levels were assessed in both normal and NF-κB knockdown HDF cells. GAPDH assured equal protein loading. Blots are representative of three identical experiments.

monodisperse to agglomerate and fall out of suspension at differential rates. Here, we observed the silver particles to settle at a much faster rate than any of the other particles. Therefore, the direct interaction between these nanoparticles and the HDF cells took place over a longer time period and with a greater concentration of particles when compared to the other particle types used in the study. These observations (combined with the increased propensity to produce ROS) led to the heightened NF-κB/ERK response in the cells after exposure to silver. Interestingly, even though titanium dioxide also induced high levels of GSSG, the NF-κB/ERK response in these cells was not elevated. This result further emphasizes that ROS production is not the only physicochemical property of nanoparticles responsible for toxicological response; instead, multiple physicochemical properties often act synergistically or antagonistically to produce a range of biological responses.

Each of the four particles exhibits different physicochemical properties, either in size, charge, or density, that correlate to other results found in this study. For example, the density of silver is much greater than that of the other particles. Quantum dots acquire a relatively neutral surface charge in media, but remain very small compared to the other three particles. Fullerols agglomerate similarly in water compared to silver, but exhibit a highly negative surface charge early, which could cause an increase in interaction with biological components, such as cell membranes.

We previously reported that quantum dots modulated the transcription factor NF-κB in HDF cells (Romoser et al., 2011). Lee et al. found that upregulation of ERK1/2 occurred in monocytes, THC-1 cells, and BALB/c mice after exposures to CdSe/ZnS quantum dots (Lee et al., 2009). There are conflicting data in the literature reporting both pro- and anti-oxidant properties after fullerol exposures. C60 fullerenes have been shown to be toxic to HDF cells, but hydroxylated fullerenes have not been tested in dermal cells (Sayes et al., 2004, 2005). As for silver, Rolla et al. found in a multi-nanoparticle study assessing possible modulation of many cellular signaling pathways that silver significantly downregulated the SMAD/TGF-β pathways, but upregulated the HIF-1α pathway (Rallo et al., 2011). Titanium dioxide has been shown to modulate the NF-κB pathway in both NIH-3T3 and BAES-2B cells exposed to 10 ng/mL and 10 μg/mL, respectively (Chen et al., 2011; Ge et al., 2011). These studies tested aggregated P25 Degussa particles however, unlike the present study.

To evaluate the response to nanoparticles in normal cells, we assayed transcriptional response via a RT-PCR gene array, as well as translational activity by way of protein analysis. A theme that emerges in the immune-transcriptional profile of cells treated with any of the assayed nanoparticles is a preparation for inflammation. Those that were upregulated were pattern recognition receptors (PRRs), their signal transduction machinery, inflammatory cytokines, and their receptors. Not only was inflammation induced, but transcripts were prepared to put the cell on a hair-trigger to escalate this response. TLR messages were upregulated to survey for pathogen-associated molecular patterns (PAMPs). NF-κB message levels were up and its inhibitors levels were down. MYD88 was prepared to convey recognition of a threat by a PRR. The MAP kinase cascade was primed. The complement cascade was attenuated (via CD55/Decay-accelerating factor) in favor of general inflammation. Additionally, IL-1 message levels increased, initiating the inflammatory cascade.

In evaluating early transcription factor activity, it was evident that the MAP kinase protein ERK1/2 was upregulated very early (within a few minutes of exposure) in the case of each type of nanoparticle exposure. Phosphorylation of IκB seemed to either be concurrent with or immediately followed ERK1/2 activation. Guma et al. has recently reported that in mice NF-κB does not trigger destructive inflammation unless MAPKs (ERK and p38) are concurrently expressed (Guma et al., 2011). Silver-treated cells continued

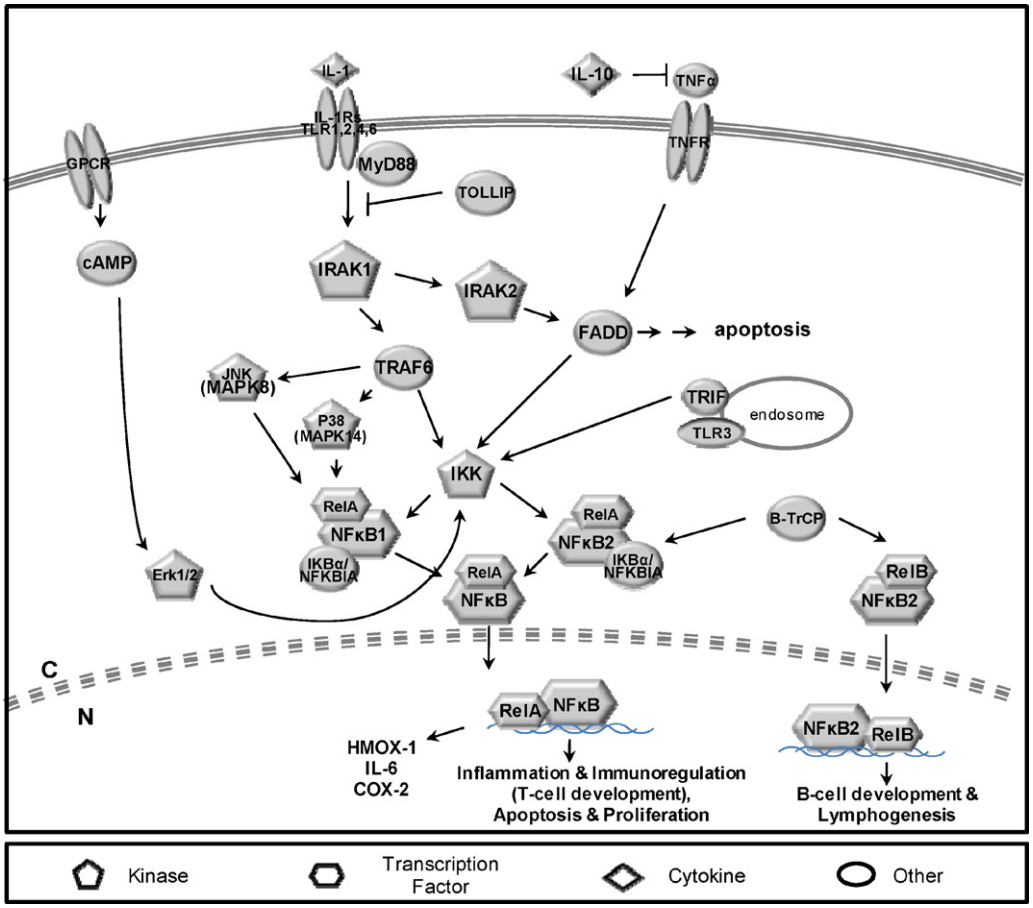

Fig. 7. Schematic. Proposed schematic of HDF NF-κB pathway and related protein involvement after nanoparticle exposures. Protein classification is denoted as such: kinase = pentagon; transcription factor = hexagon; cytokine = diamond; and other proteins = oval.

to cause upregulation of this signal transduction protein, which was possibly due to its relatively dense nature (see Table 1) and ability to settle out faster than the other particles. This density-dependent property of silver potentially exposed the cells to a greater concentration of particles over time.

To assess the extent of NF-κB dependency in cells exposed to a variety of nanoparticles, we analyzed differences in viability, antioxidant depletion, and downstream protein upregulation between knockdown and normal dermal cells. To avoid confounding toxicological effects that can occur with the use of pathway inhibitors as a method to silence a particular cellular pathway, we virally transduced our cells to specifically overexpress IκBα. In the viability assay, NF-κB knockdown cells were more resistant to death when treated with silver, fullerol, or quantum dots, however, when exposed to titanium dioxide exhibited an opposite trend. NF-κB plays a substantial role in antioxidant generation after nanoparticle exposures. Oxidative stress leads to the accumulation of glutathione disulfide (GSSG), thus GSSG measurements can be used as an indicator of cellular antioxidant protection effort.

NF-κB is known to play a role in apoptosis and may be delaying or preventing apoptosis in these nanoparticle-treated cells. Decreased cell death in knockdown cells may also be partially due to decreased nanoparticle uptake, as compared to normal HDF (data not shown). Our antioxidant data suggest that NF-κB knockdown cells are hypersensitive to insult, compared to normal cells, and allow more antioxidant involvement (increase in GSSH) to occur, possibly protecting cells from ROS generated from nanoparticles and nanoparticle–cell interaction. In other words, NF-κB may be acting to suppress some of the antioxidant response in cells exposed to nanoparticles. We observed that silver was more dense and precipitated out of the media, possibly resulting in higher exposures. That, combined with the fact that titanium dioxide was the only positively charged particle when suspended in water in the study, may be reasons for the exaggerated GSH responses with silver and titanium dioxide exposures. Furthermore, under optical microscopy, silver and titanium dioxide aggregated severely. As for differences in downstream protein expression, phosphorylation of p38 was evident after exposure to all four NP types, but was notably less severe with NF-κB knockdown. This finding coincides with earlier studies, which have shown *in vivo* that NF-κB inhibition can lead to anti-inflammatory effects (Broide et al., 2005; Greten et al., 2004). P38 is phosphorylated in response to IL-1 upregulation and further aids in activation of IL-6 (Fig. 7). Phosphorylation of p38 and JNK leads to activation of NF-κB and inflammatory response. This cascade is driven by ROS and results in downstream upregulation of inflammatory cytokines, such as IL-6, which was upregulated in the gene expression analysis at the later time point with all nanoparticles except titanium dioxide. P38 and HMOX-1 results indicate that 24 h exposure with silver and quantum dot causes partial dependency upon NF-κB for oxidative stress-related signaling. These findings, along with the IL-1α protein levels, suggest that NF-κB is responsible for controlling the majority of the inflammatory response in the dermal cells tested.

The HDF system employed here allowed for the cellular and molecular analysis of potential immunotoxicological pathways triggered by relevant exposures to chemically and physically disparate nanoparticles (Benn et al., 2011; Gopee et al., 2009; Wu et al., 2009). Such carefully chosen *in vitro* approaches should

expedite and direct subsequent *in vivo* studies to evaluate the safety of these materials.

Conflict of interest statement

None.

Acknowledgments

The authors thank Dr. Hansoo Kim and Prof. Andreas Holzenburg of the Microscopy Imaging Center at Texas A&M University for assistance with collecting the electron microscopy images. The authors also thank Prof. Yanan Tian and Sui Ke for graciously providing the NF-κB p65 and IκB-SR expression vectors. CMS also thanks The DuPont Company, the Department of Veterinary Physiology & Pharmacology, and the Product Quality Research Institute for financial support of this research. MFC thanks the Department of Veterinary Pathobiology for financial support of this research. This work was supported by the NIH through a grant to MFC (AI56963).

Appendix A. Supplementary data

Supplementary data associated with this article can be found, in the online version, at doi:10.1016/j.toxlet.2012.01.022.

References

Alivisatos, A.P., Gu, W., Larabell, C., 2005. Quantum dots as cellular probes. Annual Review of Biomedical Engineering 7, 55–76.
Benn, T., Westerhoff, P., Herckes, P., 2011. Detection of fullerenes (C60 and C70) in commercial cosmetics. Environmental Pollution 159, 1334–1342.
Broide, D.H., Lawrence, T., Doherty, T., Cho, J.Y., Miller, M., McElwain, K., McElwain, S., Karin, M., 2005. Allergen-induced peribronchial fibrosis and mucus production mediated by IkappaB kinase beta-dependent genes in airway epithelium. Proceedings of the National Academy of Sciences 102, 17723–17728.
Chen, P., Migita, S., Kanehira, K., Sonezaki, S., Taniguchi, A., 2011. Development of sensor cells using NF-κB pathway activation for detection of nanoparticle-induced inflammation. Sensors 11, 7219–7230.
Connor, E.E., Mwamuka, J., Gole, A., Murphy, C.J., Wyatt, M.D., 2005. Gold nanoparticles are taken up by human cells but do not cause acute cytotoxicity. Small 1, 325–327.
Djordjevic, A., Canadanovic-Brunet, J., Vojinovic-Miloradov, M., Bogdanovic, G., 2005. Antioxidant properties and hypothetical radical mechanism of fullerol C60(OH)24. Oxidation Communication 27, 213–218.
Duan, H., Nie, S., 2007. Cell-penetrating quantum dots based on multivalent and endosome-disrupting surface coatings. Journal of the American Chemical Society 129, 3333–3338.
Gao, X., Cui, Y., Levenson, R.M., Chung, L.W.K., Nie, S., 2004. In vivo cancer targeting and imaging with semiconductor quantum dots. Nature Biotechnology 22, 969–976.
Ge, Y., Bruno, M., Wallace, K., Winnik, W., Prasad, R.Y., 2011. Proteome profiling reveals potential toxicity and detoxification pathways following exposure of BEAS-2B cells to engineered nanoparticle titanium dioxide. Proteomics 11, 2406–2422.
Gopee, N.V., Roberts, D.W., Webb, P., Cozart, C.R., Siitonen, P.H., Latendresse, J.R., Warbitton, A.R., Yu, W.W., Colvin, V.L., Walker, N.J., Howard, P.C., 2009. Quantitative determination of skin penetration of peg-coated cdse quantum dots in dermabraded but not intact skh-1 hairless mouse skin. Toxicological Sciences 111, 37–48.
Greten, F.R., Eckmann, L., Greten, T.F., Park, J.M., Li, Z.W., Egan, L.J., Kagnoff, M.F., Karin, M., 2004. IKKbeta links inflammation and tumorigenesis in a mouse model of colitis-associated cancer. Cell 118, 285–296.
Guma, M., Stepniak, D., Shaked, H., Spehlmann, M.E., Shenouda, S., Cheroutre, H., Vicente-Suarez, I., Eckmann, L., Kagnoff, M.F., Karin, M., 2011. Constitutive intestinal NF-kB does not trigger destructive inflammation unless accompanied by MAPK activation. Journal of Experimental Medicine, doi:10.1084/jem.20110242.
Isakovic, A., Markovic, Z., Todorovic-Markovic, B., Nikolic, N., Vranjes-Djuric, S., Mirkovic, M., Dramicanin, M., Harhaji, L., Raicevic, N., Nikolic, Z., Trajkovic, V., 2006. Distinct cytotoxic mechanisms of pristine versus hydroxylated fullerene. Toxicological Sciences 91, 173–183.
Jaiswal, J.K., Mattoussi, H., Mauro, J.M., Simon, S.M., 2003. Longterm multiple color imaging of live cells using quantum dot bioconjugate. Nature Nanotechnology 21, 47–51.
Larese, F., D'Agostin, F., Crosera, M., Adami, G., Renzi, N., Bovenzi, M., Maina, G., 2009. Human skin penetration of silver nanoparticles through intact and damaged skin. Toxicology 255, 33–37.
Lee, H.M., Shin, D.M., Song, H.M., Yuk, J.M., Lee, Z.W., Lee, S.H., Hwang, S.M., Kim, J.M., Lee, C.S., Jo, E.K., 2009. Nanoparticles up-regulate tumor necrosis factor-! and CXCL8 via reactive oxygen species and mitogen-activated protein kinase activation. Toxicology and Applied Pharmacology 238, 160–169.
Livolsi, A., Busuttil, V., Imbert, V., Abraham, R.T., Peyron, J.F., 2001. Tyrosine phosphorylation-dependent activation of NF-κB: requirement for p56 LCK and ZAP-70 protein tyrosine kinases. European Journal Biochemistry 268, 1508–1515.
Tamura, M.S., Miura, T., Ikarashi, K., Watanabe, Y., Fujii, Y.M., 2010. Study on penetration of titanium dioxide (TiO(2)) nanoparticles into intact and damaged skin in vitro. Journal of Toxicological Sciences 35, 107–113.
Maynard, A.D., Kuempel, E.D., 2005. Airborne nanostructured particles and occupational health. Journal of Nanoparticle Research 7, 587–614.
Michalet, X., Pinaud, F.F., Bentolila, L.A., Tsay, J.M., Doose, S., Li, J.J., Sundaresan, G., Wu, A.M., Gambhir, S.S., Weiss, S., 2005. Quantum dots for live cells, in vivo imaging, and diagnostics. Science 307, 538–544.
Mirkov, S.M., Djordjevic, A., Andric, N.L., Andric, S.A., Kostic, T.S., Bogdanovic, G.M., Vojinovic-Miloradov, M.B., Kovacevic, R.Z., 2004. Nitric oxide-scavenging activity of polyhydroxylated fullerenol, C60(OH)24. Nitric Oxide 11, 201–207.
Monteiller, C., Tran, L., MacNee, W., Faux, S., Jones, A., Miller, B., Donaldson, K., 2007. The pro-inflammatory effects of low-toxicity low-solubility particles, nanoparticles and fine particles, on epithelial cells in vitro: the role of surface area. Occupational and Environmental Medicine 64, 609–615.
Mortensen, L.J., Oberdorster, G., Pentland, A.P., DeLouise, L.A., 2008. In vivo skin penetration of quantum dot nanoparticles in the murine model: the effect of UVR. Nano Letters 8, 2779–2787.
Müller, M., Morotti, A., Ponzetto, C., 2002. Activation of NF-κB is essential for hepatocyte growth factor-mediated proliferation and tubulogenesis. Molecular and Cellular Biology 22, 1060–1072.
Oberdorster, G., Oberdorster, E., Oberdorster, J., 2005. Nanotoxicology: An emerging discipline evolving from studies of ultrafine particles. Environmental Health Perspectives 113, 823–839.
Rallo, R., France, B., Liu, R., Nair, S., George, S., Damoiseaux, R., Giralt, F., Nel, A., Bradley, K., Cohen, Y., 2011. Self-organizing map analysis of toxicity-related cell signaling pathways for metal and metal oxide nanoparticles. Environmental Science & Technology 45, 1695–1702.
Roco, M.C., 2003. Broader societal issues of nanotechnology. Journal of Nanoparticle Research 5, 181–189.
Romoser, A.A., Chen, P.L., Berg, J.M., Seabury, C., Ivanov, I., Criscitiello, M.F., Sayes, C.M., 2011. Quantum dots trigger immunomodulation of the NFκB pathway in human skin cells. Molecular Immunology 48, 1349–1359.
Rouse, J.G., Yang, J., Ryman-Rasmussen, J.P., Barron, A.R., Monteiro-Riviere, N.A., 2007. Effects of mechanical flexion on the penetration of fullerene amino acid-derivatized peptide nanoparticles through skin. Nano Letters 7, 155–160.
Ryman-Rasmussen, J.P., Riviere, J.E., Monteiro-Riviere, N.A., 2007. Surface coatings determine cytotoxicity and irritation potential of quantum dot nanoparticles in epidermal keratinocytes. Journal of Investigative Dermatology 127, 143–153.
Rzigalinski, B.A., Strobl, J.S., 2009. Cadmium-containing nanoparticles: perspectives on pharmacology & toxicology of quantum dots. Toxicology and Applied Pharmacology 238, 280–288.
Samberg, M., Oldenburg, S., Monteiro-Riviere, N.A., 2010. Evaluation of silver nanoparticle toxicity in skin in vivo and keratinocytes in vitro. Environmental Health Perspectives 118, 407–413.
Sayes, C.M., Fortner, J.D., Guo, W., Lyon, D., Boyd, A.M., Ausman, K.D., Tao, Y.J., Sitharaman, B., Wilson, L.J., Hughes, J.B., West, J.L., Colvin, V.L., 2004. The differential cytotoxicity of water-soluble fullerenes. Nano Letters 4, 1881–1887.
Sayes, C.M., Gobin, A.M., Ausman, K.D., Mendez, J., West, J.L., Colvin, V.L., 2005. Nano-C60 cytotoxicity is due to lipid peroxidation. Biomaterials 26, 7587–7595.
Shukla, R., Bansal, V., Chaudhary, M., Basu, A., Bhonde, R.R., Sastry, M., 2005. Biocompatibility of gold nanoparticles and their endocytotic fate inside the cellular compartment: a microscopic overview. Langmuir 21, 10644–10654.
Uboldi, C., Bonacchi, D., Lorenzi, G., Hermanns, M.I., Pohl, C., Baldi, G., Unger, R.E., Kirkpatrick, C.J., 2009. Gold nanoparticles induce cytotoxicity in the alveolar type-II cell lines A549 and NCIH441. Particle & Fibre Toxicology 6.
Vandesompele, J., De Preter, K., Pattyn, F., Poppe, B., Van Roy, N., De Paepe, A., Speleman, F., 2002. Accurate normalization of real-time quantitative RT-PCR data by geometric averaging of multiple internal control genes. Genome Biology 3, 1–11.
Wang, I.C., Tai, L.A., Lee, D.D., Kanakamma, P.P., Shen, C.K.F., Luh, T.Y., Cheng, C.H., Hwang, K.C., 1991. C60 and water soluble fullerene derivatives as antioxidant against radical-initiated lipid peroxidation. Journal of Medicinal Chemistry 42, 4614–4620.
Wu, J., Liu, W., Xue, C., Zhou, S., Lan, F., Bi, L., Xu, H., Yang, X., Zeng, F.D., 2009. Toxicity and penetration of TiO_2 nanoparticles in hairless mice and porcine skin after subchronic dermal exposure. Toxicology Letters 191, 1–8.
Xia, X.R., Monteiro-Riviere, N.A., Riviere, J.E., 2010. Skin penetration and kinetics of pristine fullerenes (C60) topically exposed in industrial organic solvents. Toxicology and Applied Pharmacology 242, 29–37.
Zandi, E., 1997. The IkB kinase complex (IKK) contains two kinase subunits, IKKa and IKKb, necessary for IkB phosphorylation and NF-kB activation. Cell 91, 243–252.
Zhang, L.W., Monteiro-Riviere, N.A., 2008. Assessment of quantum dot penetration into intact, tape-stripped, abraded and flexed rat skin. Skin Pharmacology and Physiology 21, 166–180.
Zhang, L.W., Monteiro-Riviere, N.A., 2009. Mechanisms of quantum dot nanoparticle cellular uptake. Toxicological Sciences 110, 138–155.

SUPPLEMENTAL MATERIALS

Supplemental Figure 1. Experimental Design. Progression of experiments with four disparate nanoparticles tested in primary dermal fibroblasts with or without NF-κB signaling competency. Arrows relate viability, antioxidant, transcriptional and protein assays with nanoparticle concentrations cells and exposure times.

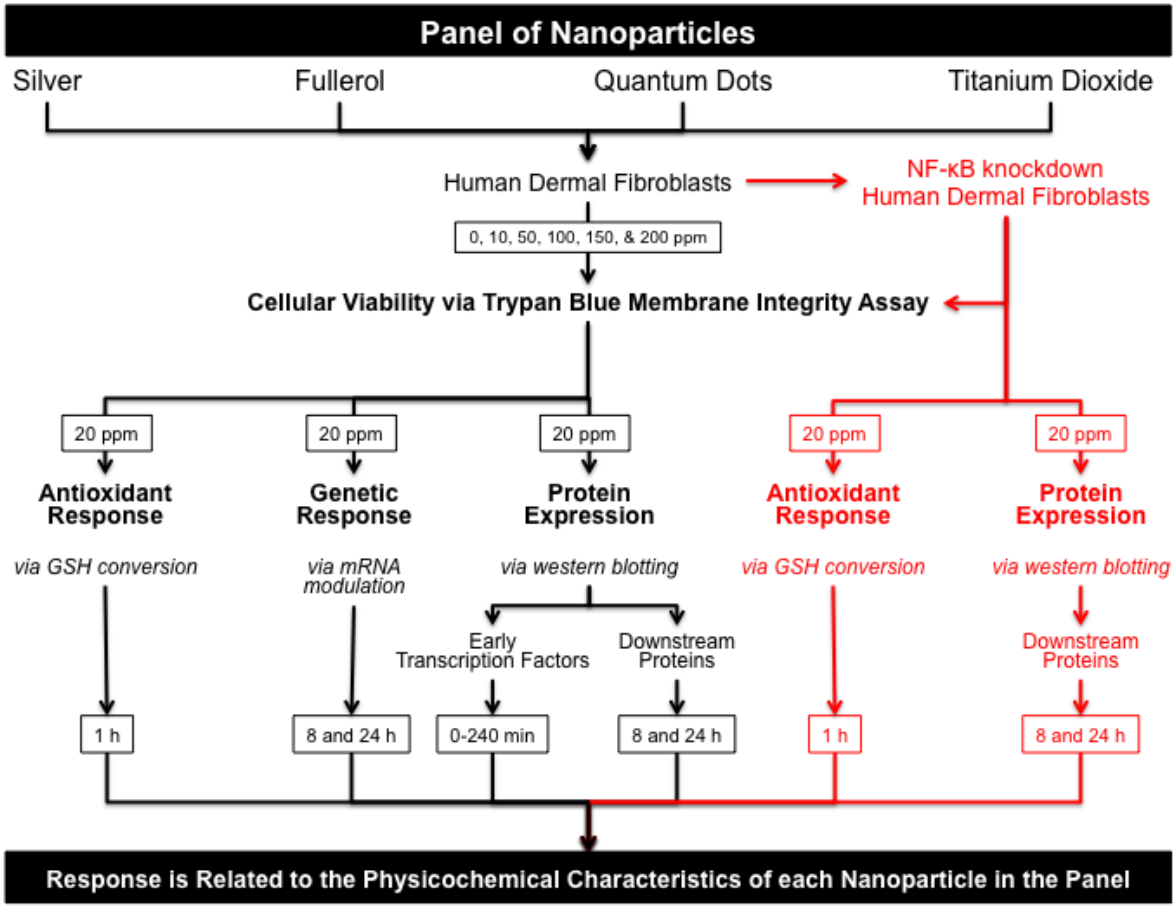

Supplemental Figure 2. Differential NF-kB expression before and after NF-kB inhibition in HDF nuclear fractions. Insertion of NF-κB inhibitor (via IκB overexpression) or empty vector, which exerts antibiotic resistance, but absence of protein overexpression capability, were all probed for p65 NF-κB expression. While both cell types show the presence of NF-κB in cytosolic fractions, IκB overexpressed cells reveal no visible NF-κB within the nucleus.

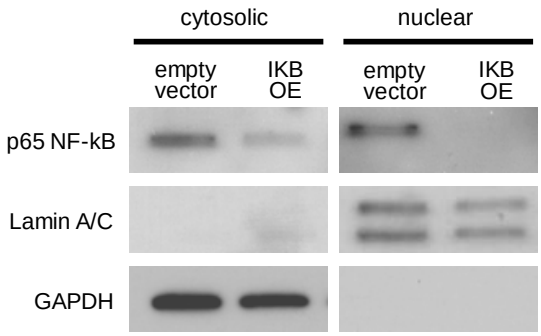

Supplemental Figure 3. Sizing profiles of the silver, fullerol, quantum dots, and titanium dioxide particles used in this study. Size was measured via dynamic light scattering spectroscopy at particle concentration of 20 ppm. The size distribution of each particle was measured and graphed as percent intensity versus hydrodynamic diameter.

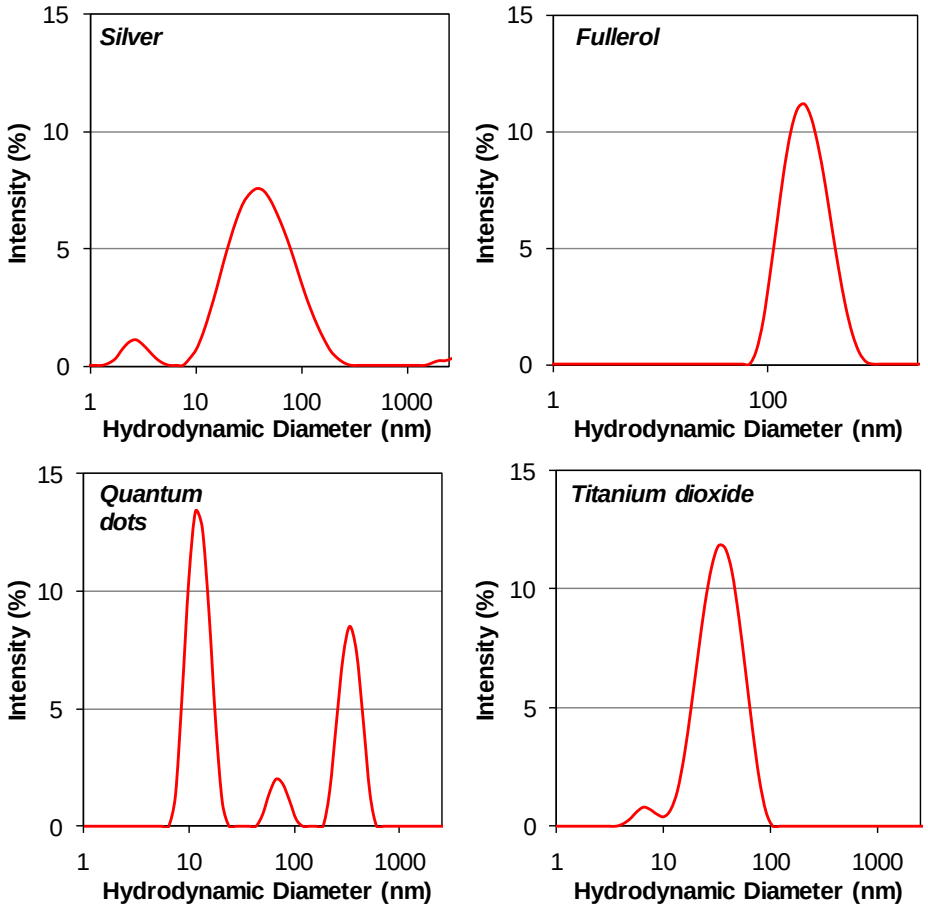

Supplemental Figure 4. Densitometric analysis was carried out to determine significance of p-IKBα and p-ERK1/2 expression differences in western blot results. Graphed results were normalized to GAPDH loading control and significance was compared between zero and all other exposure time points (zero equals untreated). *Statistically significant (p-val < 0.05).

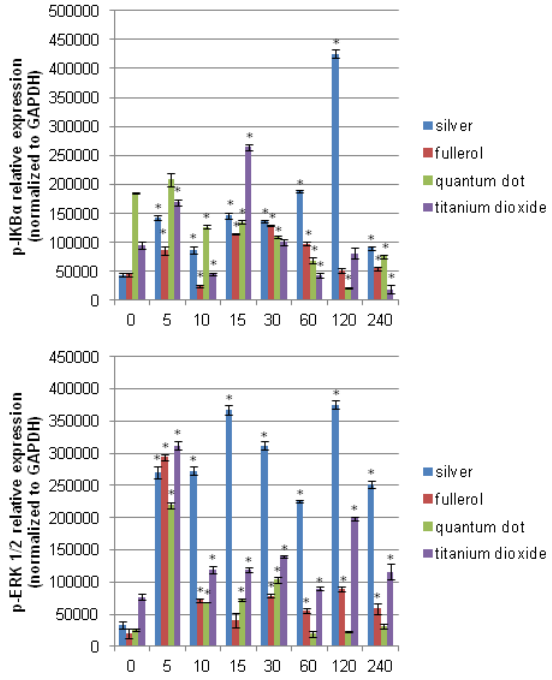

Supplemental Figure 5. Densitometric analysis was carried out to determine significance of p-p38, HMOX-1, and IL-1α expression differences in western blot results. Graphed results were normalized to GAPDH loading control. Significance between untreated and treated samples within same time point and cell type is denoted with "*" and significance between samples at same time point and treatment, but differing cell type is denoted with "†". *,† Statistically significant (p-val<0.05).

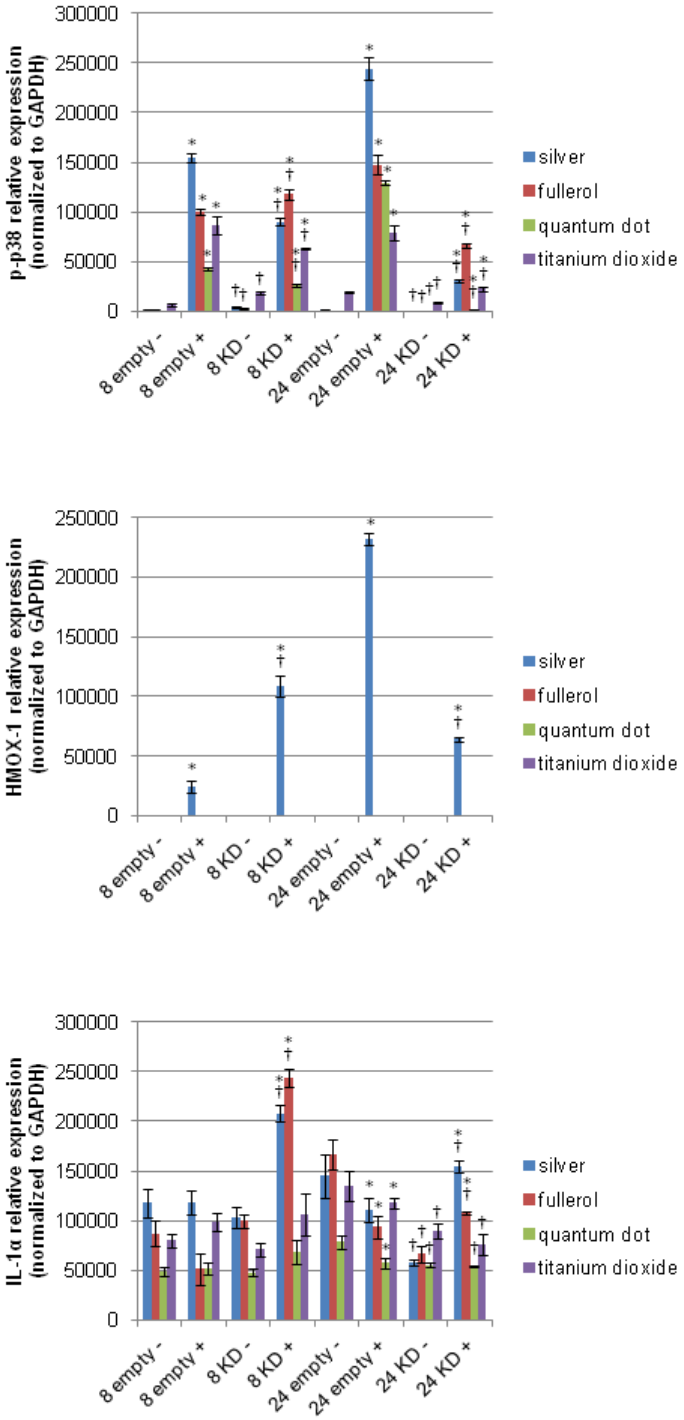

Supplemental Table 1. Complete data set of all the genes studied by real time PCR.

						8h				24h			
Pos.	**Unigene**	**GeneBank**	**Symbol**	**Description**	**Gene Name**	**Sil**	**Full**	**QD**	**TiO_2**	**Sil**	**Full**	**QD**	**TiO_2**
A01	Hs.197029	NM_000675	ADORA2A	Adenosine A2a receptor	ADORA2/RDC8	0.420	1.031	0.632	0.805	0.668		0.736	0.414
A02	Hs.494997	NM_001735	C5	Complement component 5	CPAMD4	0.787	1.211	1.013	1.025	0.822	1.765	1.122	1.45
A03	Hs.93210	NM_000562	C8A	Complement component 8, alpha polypeptide	C8A								
A04	Hs.51120	NM_004345	CAMP	Cathelicidin antimicrobial peptide	CAP18/CRAMP								
A05	Hs.2490	NM_033292	CASP1	Caspase 1, apoptosis-related cysteine peptidase (interleukin 1, beta, convertase)	ICE/IL1BC	0.678	0.798	0.867	0.9438	1.202	1.713	1.398	1.062
A06	Hs.138378	NM_001225	CASP4	Caspase 4, apoptosis-related cysteine peptidase	ICE(rel)II/ICEREL-II	1.181	0.846	0.883	1.0514	1.281	1.269	0.999	1.033
A07	Hs.303649	NM_002982	CCL2	Chemokine (C-C motif) ligand 2	GDCF-2/HC11	0.807	0.620	0.770	0.8782	0.955	0.824	1.071	1.360
A08	Hs.506190	NM_001837	CCR3	Chemokine (C-C motif) receptor 3	CC-CKR-3/CD193	0.648	0.995	0.807	0.7155	1.013	0.912	0.242	0.745
A09	Hs.163867	NM_000591	CD14	CD14 molecule	CD14					0.403	14.23	2.762	12.85
A10	Hs.1799	NM_001766	CD1D	CD1d molecule	CD1A/R3								
A11	Hs.126517	NM_000574	CD55	CD55 molecule, decay accelerating factor for complement (Cromer blood group)	CR/CROM	1.117	1.014	1.013	1.0508	1.944	2.259	1.50	0.949
A12	Hs.198998	NM_001278	CHUK	Conserved helix-loop-helix ubiquitous kinase	IKBKA/IKK-alpha	0.945	0.626	0.774	0.8375	1.757	1.592	1.283	0.770
B01	Hs.464422	NM_130386	COLEC12	Collectin sub-family member 12	CLP1/NSR2	0.653	1.129	0.933	0.9631	0.877	1.441	0.971	0.810
B02	Hs.709456	NM_000567	CRP	C-reactive protein, pentraxin-related	PTX1								
B03	Hs.593413	NM_003467	CXCR4	Chemokine (C-X-C motif) receptor 4	CD184/D2S201E								
B04	Hs.292356	NM_000397	CYBB	Cytochrome b-245, beta polypeptide	CGD/GP91-1								
B05	Hs.105924	NM_004942	DEFB4	Defensin, beta 4	DEFB-2/DEFB102								
B06	Hs.279611	NM_004406	DMBT1	Deleted in malignant brain tumors 1	GP340/muclin								
B07	Hs.203717	NM_002026	FN1	Fibronectin 1	CIG/DKFZp686F10164	0.545	1.106	0.917	1.1394	1.685	2.240	1.762	1.732
B08	Hs.517581	NM_002133	HMOX1	Heme oxygenase (decycling) 1	HO-1/HSP32	27.62	1.134	0.739	0.7956	11.15	1.789	1.475	0.627
B09	Hs.37026	NM_024013	IFNA1	Interferon, alpha 1	IFL/IFN	0.483	0.955	0.862	1.0117	1.129	1.34	1.455	2.15
B10	Hs.93177	NM_002176	IFNB1	Interferon, beta 1, fibroblast	IFB/IFF					0.861	2.598	1.521	3.281
B11	Hs.520414	NM_000416	IFNGR1	Interferon gamma receptor 1	CD119/IFNGR	0.946	1.024	0.691	0.9150	1.311	1.615	1.491	1.331
B12	Hs.634632	NM_005534	IFNGR2	Interferon gamma receptor 2 (interferon gamma transducer 1)	AF-1/IFGR2	0.908	0.759	0.866	0.8245	0.904	1.698	1.726	1.417
C01	Hs.597664	NM_001556	IKBKB	Inhibitor of kappa light polypeptide gene enhancer in B-cells, kinase beta	IKK-beta/IKK2	0.919	1.202	1.000	1.1386	1.124	2.259	1.151	1.683
C02	Hs.193717	NM_000572	IL10	Interleukin 10	CSIF/IL-10	0.785	1.233	0.502	1.3449	1.455	1.075	0.684	1.896
C03	Hs.479347	NM_001559	IL12RB2	Interleukin 12 receptor, beta 2	RP11-102M16.1	0.584	0.828	0.428	0.6424		1.041	2.123	5.595
C04	Hs.1722	NM_000575	IL1A	Interleukin 1, alpha	IL-1A/IL1	0.604	1.261	1.360	0.7911	5.126	2.258	2.374	2.181
C05	Hs.126256	NM_000576	IL1B	Interleukin 1, beta	IL-1/IL1-BETA	0.777	0.798	0.550	1.0895	4.239	1.898	1.257	2.264
C06	Hs.306974	NM_173161	IL1F10	Interleukin 1 family, member 10 (theta)	FIL1-theta/FKSG75								
C07	Hs.516301	NM_012275	IL1F5	Interleukin 1 family, member 5 (delta)	FIL1/FIL1(DELTA)								
C08	Hs.278910	NM_014440	IL1F6	Interleukin 1 family, member 6 (epsilon)	FIL1/FIL1(EPSILON)								
C09	Hs.166371	NM_173205	IL1F7	Interleukin 1 family, member 7 (zeta)	FIL1/FIL1(ZETA)	0.281	1.324	0.967	0.5218	29.49	14.72	13.95	36.11
C10	Hs.278909	NM_173178	IL1F8	Interleukin 1 family, member 8 (eta)	FIL1/FIL1-(ETA)	2.429	1.178	0.837	2.1693				
C11	Hs.211238	NM_019618	IL1F9	Interleukin 1 family, member 9	IL-1F9/IL-1H1	0.393		1.468			5.483	1.837	
C12	Hs.701982	NM_000877	IL1R1	Interleukin 1 receptor, type I	CD121A/D2S1473	0.650	0.825	0.857	0.9307	0.629	1.555	1.165	0.960
D01	Hs.25333	NM_004633	IL1R2	Interleukin 1 receptor, type II	CD121b/IL1RB	1.009	0.237	0.466	0.2387	0.634	0.617	0.241	
D02	Hs.478673	NM_002182	IL1RAP	Interleukin 1 receptor accessory protein	C3orf13/IL-1RAcP	0.916	1.664	1.027	1.3645	1.987	2.388	1.327	2.130
D03	Hs.675519	NM_017416	IL1RAPL2	Interleukin 1 receptor accessory protein-like 2	IL-1R9/IL1R9	0.601	0.989	1.390	0.6888		0.514	0.910	1.413
D04	Hs.659863	NM_003854	IL1RL2	Interleukin 1 receptor-like 2	IL1R-rp2/IL1RRP2	1.112	0.653	0.991	0.5583	0.402	1.637	1.086	1.204
D05	Hs.81134	NM_000577	IL1RN	Interleukin 1 receptor antagonist	ICIL-1RA/IL-1ra3	0.837	1.284	0.499	0.4624				
D06	Hs.654458	NM_000600	IL6	Interleukin 6 (interferon, beta 2)	BSF2/HGF	1.515	0.814	0.878	0.7693	2.644	2.418	1.575	1.080
D07	Hs.522819	NM_001569	IRAK1	Interleukin-1 receptor-associated kinase 1	IRAK/pelle	0.889	1.196	1.180	1.8760	2.705	2.290	3.198	3.198
D08	Hs.449207	NM_001570	IRAK2	Interleukin-1 receptor-associated kinase 2	IRAK-2	0.768	0.580	0.700	0.6441	1.389	0.630	0.739	0.820
D09	Hs.436061	NM_002198	IRF1	Interferon regulatory factor 1	IRF-1/MAR	0.756	1.298	0.819	1.2068	0.765	1.544	1.454	1.813
D10	Hs.72938	NM_002289	LALBA	Lactalbumin, alpha-	MGC138521								
D11	Hs.154078	NM_004139	LBP	Lipopolysaccharide binding protein	MGC22233								
D12	Hs.529517	NM_002343	LTF	Lactotransferrin	GIG12/HLF2								
E01	Hs.660766	NM_015364	LY96	Lymphocyte antigen 96	MD-2/MD2	0.841	1.045	0.847	1.0367	1.817	1.237	1.093	0.899
E02	Hs.524579	NM_000239	LYZ	Lysozyme (renal amyloidosis)	LZM/lysozyme	0.273		0.988					1.158
E03	Hs.485233	NM_001315	MAPK14	Mitogen-activated protein kinase 14	CSBP1/CSBP2	0.728	1.054	0.920	1.1487	1.263	1.582	1.480	1.509
E04	Hs.138211	NM_002750	MAPK8	Mitogen-activated protein kinase 8	JNK/JNK1	0.770	0.849	0.940	0.9371	1.557	1.809	1.575	1.626
E05	Hs.407995	NM_002415	MIF	Macrophage migration inhibitory factor (glycosylation-inhibiting factor)	GIF/GLIF	0.935	1.197	0.998	1.1617	1.669	1.350	1.085	0.904
E06	Hs.82116	NM_002468	MYD88	Myeloid differentiation primary response gene (88)	MYD88D	0.769	1.181	1.180	1.3350	1.249	1.742	1.447	1.784
E07	Hs.474781	NM_000631	NCF4	Neutrophil cytosolic factor 4, 40kDa	NCF/P40PHOX		1.155		1.1129				
E08	Hs.654408	NM_003998	NFKB1	Nuclear factor of kappa light polypeptide gene enhancer in B-cells 1	DKFZp686C01211/EBP-1	0.896	0.901	0.947	0.9023	1.470	1.298	1.163	0.802
E09	Hs.73090	NM_002502	NFKB2	Nuclear factor of kappa light polypeptide gene enhancer in B-cells 2 (p49/p100)	LYT-10/LYT10	0.717	1.292	1.136	1.2886	1.176	1.76	2.209	1.356
E10	Hs.81328	NM_020529	NFKBIA	Nuclear factor of kappa light polypeptide gene enhancer in B-cells inhibitor, alpha	IKBA/MAD-3	1.116	1.034	0.954	0.9956	1.046	1.113	1.113	0.651
E11	Hs.574741	NM_021209	NLRC4	NLR family, CARD domain containing 4	CARD12/CLAN	0.366	0.520	0.813	0.5262	1.910	2.593	1.993	0.552
E12	Hs.709191	NM_000625	NOS2	Nitric oxide synthase 2, inducible	HEP-NOS/INOS								

F01	Hs.137583	NM_005091	PGLYRP1	Peptidoglycan recognition protein 1	PGLYRP/PGRP					7.073	11.47	4.892	9.837
F02	Hs.282244	NM_052890	PGLYRP2	Peptidoglycan recognition protein 2	HMFT0141/PGLYRPL								
F03	Hs.348266	NM_052891	PGLYRP3	Peptidoglycan recognition protein 3	PGRP-Ialpha/PGRPIA			0.334					
F04	Hs.2164	NM_002704	PPBP	Pro-platelet basic protein (chemokine (C-X-C motif) ligand 7)	B-TG1/Beta-TG								
F05	Hs.224698	NM_000312	PROC	Protein C (inactivator of coagulation factors Va and VIIIa)	PC/PROC1								
F06	Hs.709174	NM_000952	PTAFR	Platelet-activating factor receptor	PAFR		1.887						
F07	Hs.19413	NM_005621	S100A12	S100 calcium binding protein A12	CAAF1/CAGC								
F08	Hs.525557	NM_000295	SERPINA1	Serpin peptidase inhibitor, clade A (alpha-1 antiproteinase, antitrypsin), member 1	A1A/A1AT	1.225	1.594	1.016	1.0192	0.769	1.553		1.961
F09	Hs.414795	NM_000602	SERPINE1	Serpin peptidase inhibitor, clade E (nexin, plasminogen activator inhibitor type 1), member 1	PAI/PAI-1	0.788	1.092	0.797	1.0791	0.976	1.473	0.883	1.296
F10	Hs.253495	NM_003019	SFTPD	Surfactant protein D	COLEC7/PSP-D	0.410	0.582	0.740	0.5061	146.5	170.3	110.0	404.2
F11	Hs.645227	NM_000660	TGFB1	Transforming growth factor, beta 1	CED/DPD1	0.871	1.033	1.008	1.1351	0.935	1.548	1.617	1.765
F12	Hs.654532	NM_003263	TLR1	Toll-like receptor 1	CD281/DKFZp547I061 0						2.639	0.749	0.799
G01	Hs.120551	NM_030956	TLR10	Toll-like receptor 10	CD290								
G02	Hs.519033	NM_003264	TLR2	Toll-like receptor 2	CD282/TIL4					0.634	1.213	1.140	
G03	Hs.657724	NM_003265	TLR3	Toll-like receptor 3	CD283	1.169	2.587	1.795	1.9203	0.744	1.416	1.379	0.837
G04	Hs.174312	NM_138554	TLR4	Toll-like receptor 4	ARMD10/CD284	1.134	0.852	0.930	0.9944	1.089	1.005	0.948	0.872
G05	Hs.662185	NM_006068	TLR6	Toll-like receptor 6	CD286	1.085	1.841	1.361	0.9697	1.278	1.866	1.377	1.277
G06	Hs.660543	NM_138636	TLR8	Toll-like receptor 8	CD288								
G07	Hs.87968	NM_017442	TLR9	Toll-like receptor 9	CD289								
G08	Hs.241570	NM_000594	TNF-α	Tumor necrosis factor (TNF superfamily, member 2)	DIF/TNF-alpha					0.444	0.535	0.356	0.397
G09	Hs.279594	NM_001065	TNFRSF1A	Tumor necrosis factor receptor superfamily, member 1A	CD120a/FPF	0.895	1.105	0.902	1.0035	0.836	1.133	0.860	0.366
G10	Hs.368527	NM_019009	TOLLIP	Toll interacting protein	IL-1RAcPIP	1.155	0.707	1.016	0.7538	1.389	1.320	1.216	0.645
G11	Hs.591983	NM_004620	TRAF6	TNF receptor-associated factor 6	MGC:3310/RNF85	1.133	0.773	0.979	0.7916	1.377	1.578	1.376	0.923
G12	Hs.283022	NM_018643	TREM1	Triggering receptor expressed on myeloid cells 1	TREM-1	1.284			3.535				